Babeş-Bolyai University
Faculty of Physics

Scientific Report for Project
PN-II-RU-TE-2014-4-2360

January - December 2016

Project Director: Dr. Albert Takacs

December 2016

Contents

1. Project Objectives 3
2. Phase 2: January - December 2016 4
2.1. Results Summary for Phase 2: January - December 2016 4
2.1.1. Effect of the Ar deposition pressure on the structural properties of Cr(150 nm)/Sm-Co(30 nm)/Cr(5 nm) multilayers 4
2.1.2. Influence of the $Fe_{65}Co_{35}$ Thickness on the Structural, Electronic and Magnetic properties of Cr/$Fe_{65}Co_{35}$ bilayers 6
2.2. Conclusions for Phase 2: January - December 2016 14
2.3. References 15

1. Project Objectives

This project intends to approach the study of the exchange spring concept in thin films experimentally as well as theoretically. An important aspect is the dimensionality effect, the variation of magnetic moments at surfaces and interfaces being correlated with magnetic anisotropy. Therefore, the influence of the deposition conditions of both hard and soft magnetic films is important in order to successfully prepare and investigate exchange coupled multilayer films. The project has two main objectives.

The first objective is focused on the preparation and study of hard and soft magnetic films. The effects of preparation conditions on the structural, microstructural and magnetic properties of hard and soft magnetic films will be investigated (Ar pressure, deposition temperature, sputtering power, substrate type, substrate thickness, and film thickness). Fully relativistic band structure calculations will also be employed in order to have a clear input for the experimental part of the project.

The second objective proposes the preparation and study of exchange coupled multilayer systems based on the results obtained after accomplishing the first objective. Fully epitaxial $SmCo_5$/Fe(Co)/$SmCo_5$ multilayer films are to be prepared, in which the easy magnetization axis of both hard magnetic layers is aligned along one single direction. The interlayer exchange coupling will be studied by hysteresis measurements and by DC-demagnetizing loops for different thicknesses of the soft magnetic thin film. In order to support the experimental observations, electronic structure calculations will also be performed. A successful coupling together with the optimum texture provided by the epitaxial growth of the hard magnetic thin film would lead to excellent magnetic properties. We are aiming for small thicknesses for the soft magnetic material (raging from a few nm) in order to get fully coupled layers. Hysteresis curves with high coercivity and large remanence are expected.

2. Phase 2: January - December 2016

2.1. Results Summary for Phase 2: January - December 2016

In this section, we will present the results regarding hard and soft magnetic films. In Phase 2 we focused our attention on studying the structural and magnetic properties of hard and soft magnetic multilayers. Band structure calculations were employed in order to support the experimental observations. The obtained results were submitted for publication in ISI indexed articles [1,2] and presented at international conferences [3-6]. In subsection 2.1.1 we discuss the effect of the partial Ar pressure on the structural properties of Cr/Sm-Co multilayers. In subsection 2.1.2, we present the influence of $Fe_{65}Co_{35}$ layer thickness on the structural, electronic and magnetic properties of $Cr/Fe_{65}Co_{35}$ bilayers.

2.1.1. Effect of the Ar deposition pressure on the structural properties of Cr(150 nm)/Sm-Co(30 nm)/Cr(5 nm) multilayers

The Ar deposition pressure is a very important parameter regarding the preparation of hard magnetic layers. By varying this parameter we can trigger the complexity of the Sm-Co phase. In Phase 2 we continued the research which begun in Phase 1. If in the first phase we focused our attention on very thin Sm-Co layers (around 5 nm thick), in the second phase we chose to study thicker Cr/Sm-Co layers.

Cr(150 nm)/Sm-Co(30 nm)/Cr(5 nm) multilayers were prepared. The Sm-Co layers were prepared by DC magnetron sputtering of a 1:5 Sm-Co target on a $Si(100)/SiO_2$ substrate coated with 150 nm of Cr. The Cr buffer layer forms an adequate base for growing Sm-Co by helping to maintain the in-plane anisotropy of $SmCo_5$. Also, the Cr layer prevents the Sm atoms from interacting with the thermally oxidized Si substrate. The Cr and Sm-Co layers were deposited in a base pressure of 7×10^{-7} mbar. The deposition temperature of the Cr seed layer was 490ºC, while the Sm-Co and Cr cap layers were deposited at room temperature. The deposition rates were 1.1 Å/s for Cr layers and 8.7 Å/s for Sm-Co layers. Three Cr/Sm-Co/Cr films were prepared, the Ar partial pressure for the Sm-Co deposition being 1.4×10^{-3} mbar, 2.9×10^{-3} mbar and 5.9×10^{-3} mbar respectively. The Ar partial pressure value was kept constant at 4.5×10^{-3} mbar during all of the Cr layer depositions. For each Sm-Co thin film that was obtained, a 5 nm cap layer was deposited from a pure solid Cr target (99.9% purity) in order to protect the film from oxidation. After deposition, the films were annealed under vacuum at a temperature of 600ºC.

The crystal structure of the hard magnetic multilayers was investigated using a Bruker D8 Advance diffractometer with Cu Kα radiation and Bragg-Brentano focusing

geometry. The X-ray diffraction patterns for the as-deposited multilayers are shown below. The obtained Cr seed layers are textured polycrystalline films. The intensity ratio between the (110) and (211) peaks of the deposited Cr layer is around half of the value found for bulk Cr. This shows that the Cr seed layer is textured along the (211) direction. All of the deposited Sm-Co layers are phase mixtures comprised of the $SmCo_5$ and Sm_2Co_{17} phases. It is worthwhile to note that with increasing pressure, the intensity of the Sm_2Co_{17} XRD peaks increases relative to the Cr and $SmCo_5$ peaks. This means that at higher deposition pressures more Co atoms reach the substrate than Sm atoms, which changes the Sm-Co layer stoichiometry.

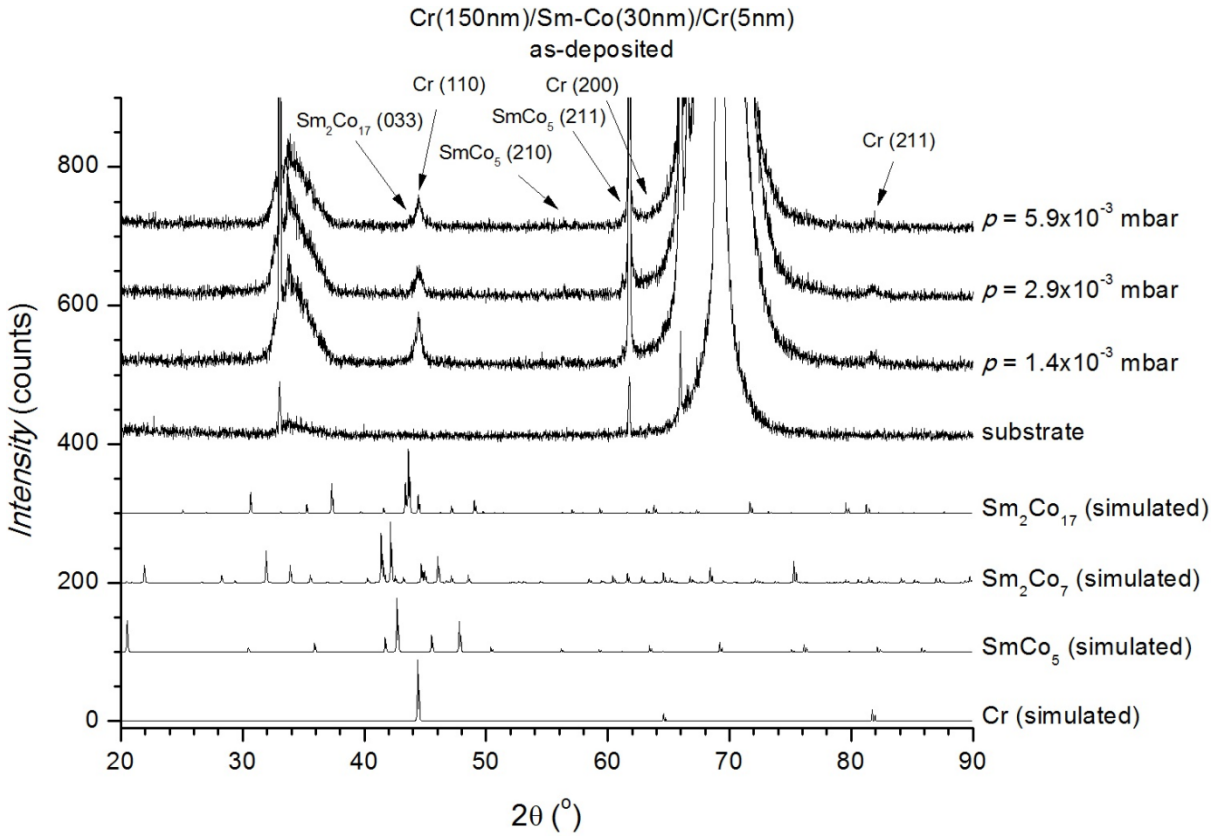

Figure 1. X-ray diffraction patterns of the as-obtained Cr(150 nm)/Sm-Co(30 nm)/Cr(5 nm) multilayers deposited at different Ar pressures. The XRD pattern of the substrate and the theoretical patterns of Cr, $SmCo_5$, Sm_2Co_7 and Sm_2Co_{17} are also shown for comparison.

The X-ray diffraction pattern of the multilayer deposited at an Ar partial pressure of 1.4 x 10^{-3} mbar and annealed in vacuum at 600ºC is shown below. In addition to the $SmCo_5$ peaks, the Sm_2Co_{17} (113) and (312) peaks become visible in the XRD patterns after annealing. It is possible that annealing at 600ºC leads to the decomposition of the $SmCo_5$ phase into the neighboring Sm_2Co_7 and Sm_2Co_{17} phases. In order to obtain the $SmCo_5$ phase, annealing at higher temperatures may be required.

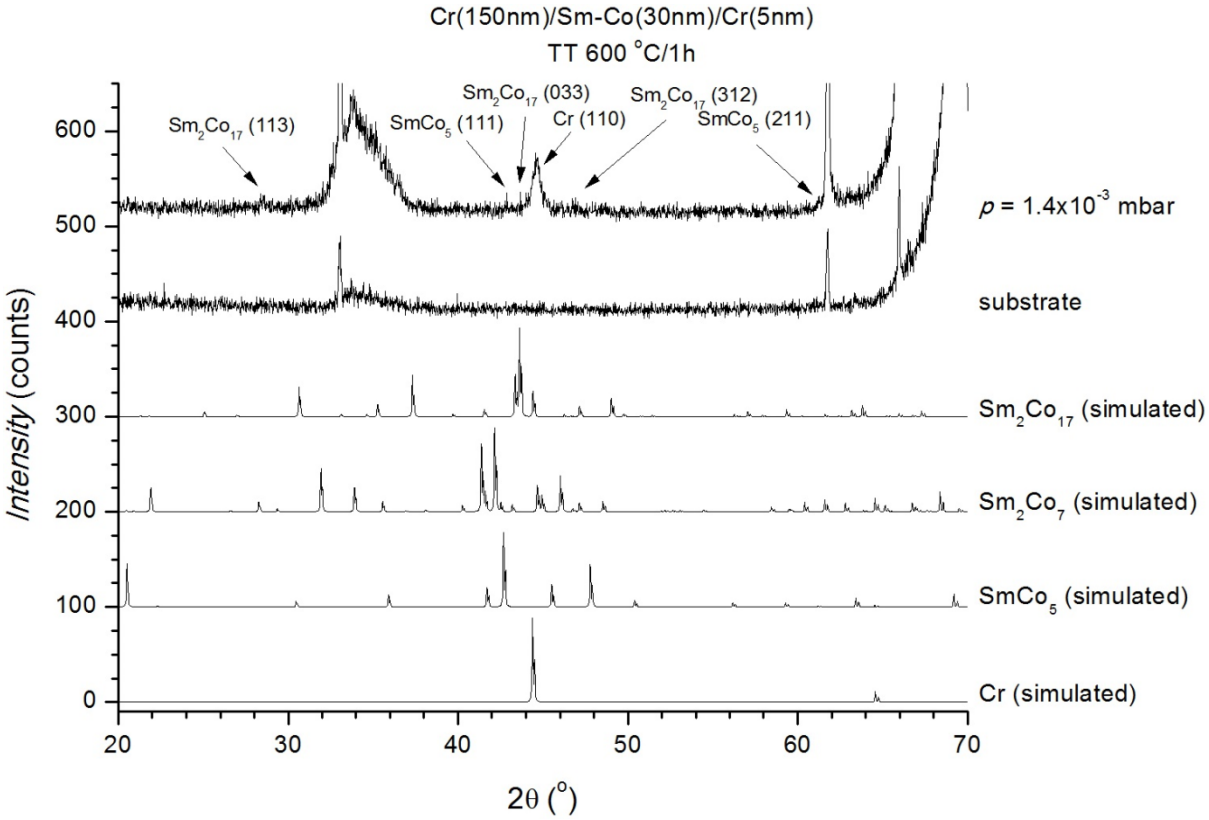

Figure 2. X-ray diffraction pattern of the Cr(150 nm)/Sm-Co(30 nm)/Cr(5 nm) sample deposited at 1.4 x 10^{-3} mbar and annealed at 600ºC. The XRD pattern of the substrate and the theoretical patterns of Cr, $SmCo_5$, Sm_2Co_7 and Sm_2Co_{17} are also shown for comparison.

In the next phase, thermal treatments at higher temperatures will be performed in order to obtain a single-phase $SmCo_5$ layer. We will deposit hard magnetic multilayers on different substrates (such as glass, Cr or MgO) in order to obtain both polycristalline and epitaxial multilayers. In order to study the magnetic properties of the multilayers, magnetic measurements will be performed by using a vibrating sample magnetometer in the 4-300 K temperature range in applied fields up to 12 T.

2.1.2. Influence of the $Fe_{65}Co_{35}$ Thickness on the Structural, Electronic and Magnetic properties of Cr/$Fe_{65}Co_{35}$ bilayers

Chromium (Cr) is an itinerant antiferromagnet which exhibits many interesting magnetic properties. Unlike common antiferromagnets, such as CoO and MnO, where we have an ordering of localized moments, Cr is an itinerant spin density wave (SDW) antiferromagnet [7]. Bulk Cr orders antiferromagnetically in an incommensurate spin-density wave (ISDW), where the magnitude of the sublattice spins, $\mathbf{S}_{AF}$ is modulated sinusoidally [8,9]. Parker et al. [8] describe the ISDW through a wave vector **Q**, which has a wavelength $\lambda = 2\pi/|\mathbf{Q}|$, which is incommensurate with the periodicity of the crystal lattice. Two ISDW

phases are present below the Neel temperature, T_N: a high temperature transverse phase, where $\mathbf{Q} \perp \mathbf{S}_{AF}$, and a low temperature longitudinal phase, where $\mathbf{Q} \parallel \mathbf{S}_{AF}$ [8,9]. The two phases are separated by a spin-flip transition temperature T_{SF} = 123 K [9]. Neutron diffraction studies have shown that the ISDW wave vector **Q** lies along the (100) direction and the wavelength increases with temperature from 60 Å at 10 K to 78 Å at 311 K [9,10]. In thin films, the "finite-size" confinement leads to interesting behaviors very different from the bulk, the most important being giant magnetoresistance and exchange bias in AFM/FM multilayer systems [11-13].

Due to its scientific relevance and technological application possibilities in magnetic storage, exchange bias is receiving increasing attention [14-17]. It was shown that the exchange bias at the AFM/FM interface is significantly influenced by both the ISDW in the antiferromagnet and frustration effects at the interface [7,17]. For very thin films, the frustration effects at the interface dominate the AFM structure, while for thicker films, the Cr layer becomes gradually "bulk-like" [17]. In Cr/Fe multilayers, the transition from "bulk-like" to "finite-size" was reported to be around 1100 Å [8]. Exchange bias in Cr/FM multilayers was studied in both epitaxial and polycrystalline systems, where the ferromagnetic material was Fe, Co, or Permalloy [7,8,17,18]. These studies showed that the exchange coupling at the AFM/FM interface is influenced by the Cr layer thickness as well as the ferromagnetic layer thickness. In the present research project, Cr is used as a seed layer for our polycrystalline films mainly due to its good lattice mismatch with both $SmCo_5$ and $Fe_{65}Co_{35}$, materials which we will later use to prepare exchange coupled multilayers. Also, Cr is used as a protective layer, preventing the oxidation of the top layer containing $SmCo_5$ (capping layer), and the diffusion of oxygen from the SiO_2 substrate (underlayer). Therefore, it is important to understand the effect of the ferromagnetic layer thickness on the magnetic properties of $Cr/Fe_{65}Co_{35}$ bilayers.

Bilayers were deposited at room temperature using DC magnetron sputtering in the $Cr(100\ nm)/Fe_{65}Co_{35}(25\text{-}100\ nm)$ configuration onto Si(100) substrates with a 100 nm SiO_2 layer. The base pressure was 7×10^{-7} mbar. The Ar pressure during deposition was kept at 4.5×10^{-3} mbar for Cr and 2×10^{-3} mbar for $Fe_{65}Co_{35}$. The sputtering power for all of the samples was 30 W. The layer thicknesses and rates were measured during sample deposition using an Inficon SQM-160 rate/thickness monitor previously calibrated by x-ray reflectometry (XRR) measurements. The XRR and XRD measurements were performed using a Bruker D8 Advance diffractometer with Cu K_α radiation. The crystal structure of the films was investigated through grazing incidence XRD scans. Magnetic measurements were performed using a vibrating sample magnetometer in the temperature range 4-300 K.

The film thicknesses measured during the sample deposition are shown in Table 2. The obtained layer thickness values are close to the desired values for both the single Cr layer sample and the multilayer Cr/Fe-Co configurations.

Table 1. Measured thickness values during deposition for the Cr single layer and Cr/Fe-Co multilayer configurations.

Desired configuration	Measured thickness values	
	t_{Cr} (nm)	$t_{Fe\text{-}Co}$ (nm)
Cr(100 nm)	99	-
Cr(100 nm)/$Fe_{65}Co_{35}$(100 nm)	96	102
Cr(100 nm)/$Fe_{65}Co_{35}$(50 nm)	96	52
Cr(100 nm)/$Fe_{65}Co_{35}$(25 nm)	95	25

The X-ray reflectivity (XRR) measurement results are shown in Figure 6. It can be observed that there are no oscillations in reflectivity for any of the bilayer samples. The same behavior was found in the single layer sample containing 100 nm of Cr. This behavior is an indicative of a rough Cr surface, and consequently a rough interface when Cr/Fe-Co multilayers are prepared. A surface roughness of around 3-4 nm was determined from XRR measurements, which is unavoidable in polycrystalline sputtered films [7].

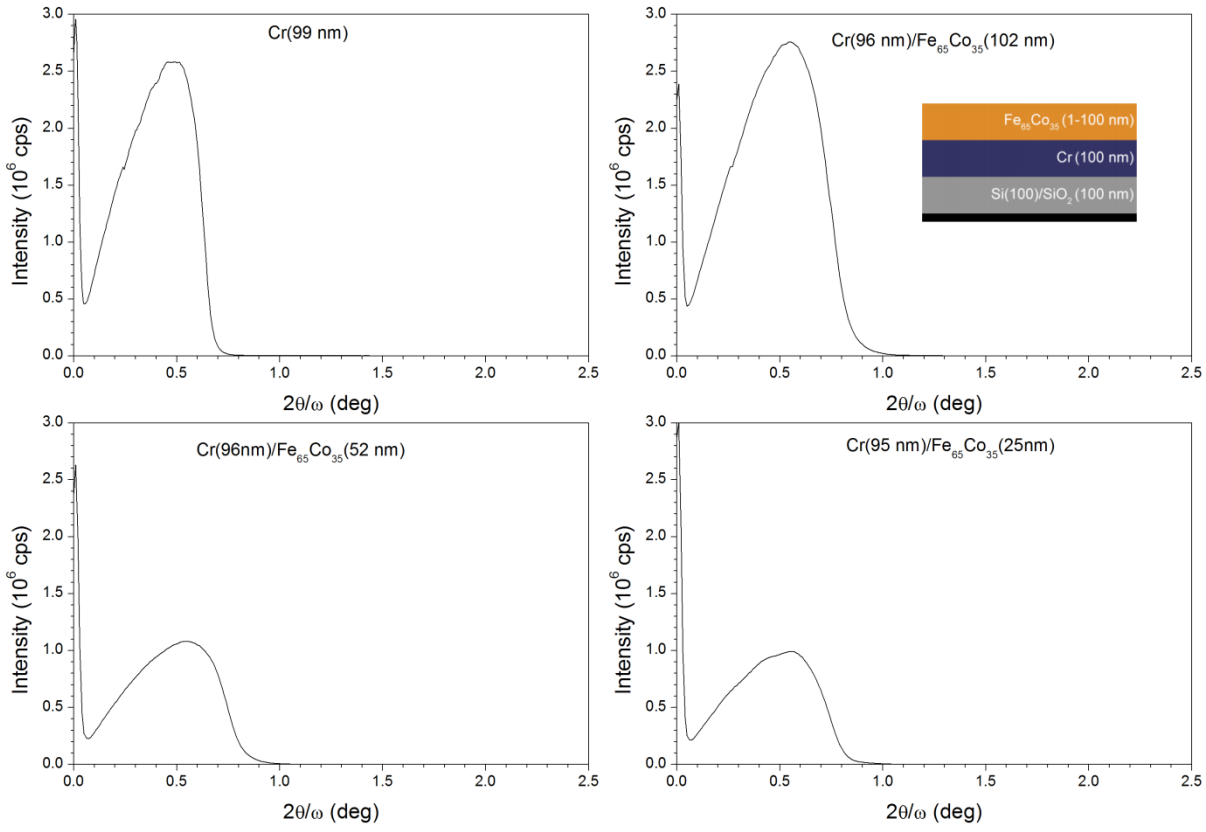

Figure 3. X-ray reflectivity curves for all of the prepared Cr/Fe-Co multilayer samples, along with the XRR curve for the sample containing only one Cr layer.

The grazing incidence X-ray diffraction patterns are shown in Figure 7. The grazing incidence scans were performed as 2θ detector scans at fixed source θ values of 0.8 and 1.5 degrees. In the Cr(99 nm) sample only the (110) Cr reflection can be identified, meaning

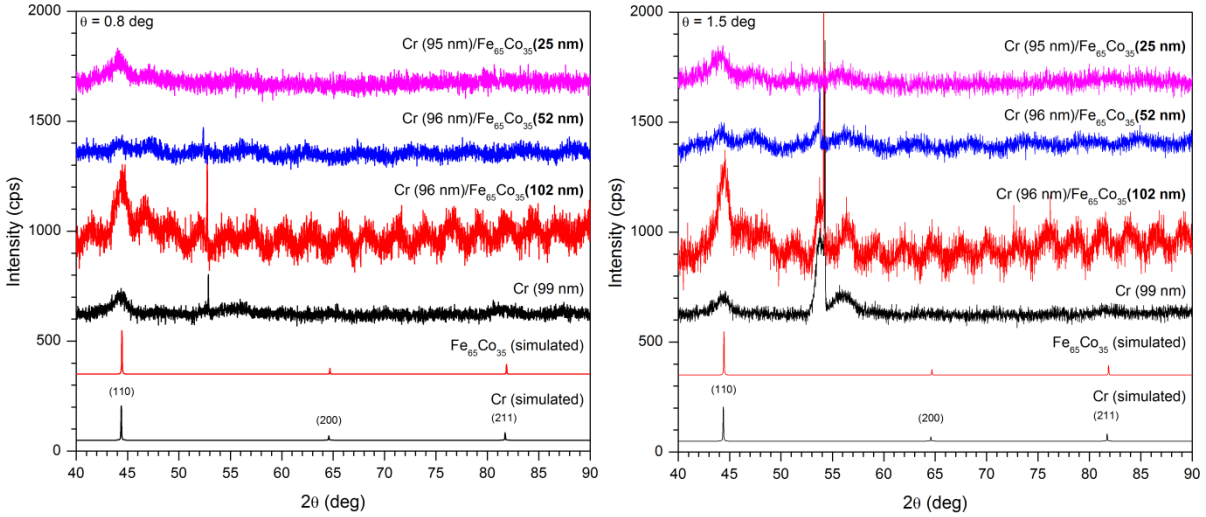

Figure 4. Grazing incidence XRD patterns for all of the obtained samples at fixed θ values of 0.8 and 1.5 degrees. The simulated XRD patterns of Cr and $Fe_{65}Co_{35}$ are shown for comparison.

that the Cr underlayer is textured along the (110) direction. The other reflections were attributed to the Si substrate. Texturing along the (110) direction is common for polycrystalline Cr films deposited at room temperature and low sputtering power [20]. The multilayer Cr/Fe-Co samples also show only the (110) Cr reflection. The (110) $Fe_{65}Co_{35}$ reflection superimposes on the (110) Cr peak, therefore it is difficult to separate the two contributions. However, considering that both Cr and $Fe_{65}Co_{35}$ have the same crystal structure with a very small mismatch between the lattice parameters, we can safely say that the $Fe_{65}Co_{35}$ layer grows in tune with the Cr layer. Therefore, we can conclude that the multilayer samples contain both crystalline Cr and $Fe_{65}Co_{35}$, with a lattice parameter of 2.88 Å for both the Cr and $Fe_{65}Co_{35}$ layers.

In order to support the experimental observations, electronic structure calculations have been performed. The theoretical calculations were performed in order to clarify the evolution of the magnetic properties of the Fe and Fe-Co films as a function of thickness.The correlation between the structure and magnetism for 3d metals has been investigated using the tight-binding-KKR (Korringa-Kohn-Rostoker) band structure calculation method [21]. The SPR-TB-KKR program package allows dealing with nearly any 3D- and 2D-systems making use of the screened or tight binding KKR formalism [22]. A separate program allows in addition to deal with commensurate 0D-subsystems embedded in a 3D- or 2D-host system. The calculations are done in spin-polarized fully-relativistic mode, using CPA alloy theory, in

ferromagnetic and antiferromagnetic spin configuration. The local spin density approximation (LSDA) for the exchange-correlation energy using the Vosko, Wilk and Nusair (VWN) parameterization was used [23].

The system of 1 ML (one monolayer) of Fe/Cr(001) has been constructed, as can be seen in Figure 8. The experimental lattice parameter of Cr has been used for calculations. The layer-resolved spin and orbital magnetic moments for this system can be seen in Table 3. The Fe spin magnetic moment is close to the bulk-value (2.2 μ_B) and an increased orbital moment (0.1 μ_B), suggesting an increased anisotropy compared with bulk. The Cr underlayers show an SDW behaviour with decreasing amplitude by increasing the layer depth.

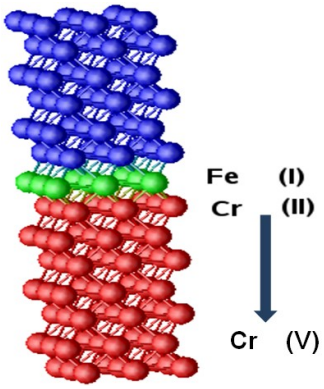

Figure 5. The configuration of the Fe/Cr(001) layers.

Table 2. The layer-resolved spin and orbital magnetic moments for the configuration Fe/Cr(001).

Layer	$m_s(\mu_B)$	$m_l(\mu_B)$
Fe (I)	2.19	0.10
Cr (II)	-1.15	0.005
Cr (III)	1.05	0.00
Cr (IV)	-0.79	0.00
Cr (V)	0.53	0.00

Table 3. The layer-resolved spin and orbital magnetic moments for the configuration consisting of 1, 2, and 4 ML of $Fe_{0.5}Co_{0.5}$/Cr(001).

Layer	1 ML $Fe_{0.5}Co_{0.5}$/Cr(001)		2 ML $Fe_{0.5}Co_{0.5}$/Cr(001)		4 ML $Fe_{0.5}Co_{0.5}$/Cr(001)	
	$m_s(\mu_B)$	$m_l(\mu_B)$	$m_s(\mu_B)$	$m_l(\mu_B)$	$m_s(\mu_B)$	$m_l(\mu_B)$
Fe (I)	-	-	-	-	2.86	0.12
Co (I)	-	-	-	-	1.75	0.14
Fe (II)	-	-	-	-	2.47	0.06
Co (II)	-	-	-	-	1.65	0.09
Fe (III)	-	-	2.89	0.12	2.61	0.07
Co (III)	-	-	1.75	0.14	1.62	0.11
Fe (IV)	2.42	0.08	1.87	0.05	2.00	0.05
Co (IV)	-0.69	-0.04	1.10	0.06	1.03	0.06
Cr (V)	-0.85	0.00	-0.27	0.00	-0.25	0.00
Cr (VI)	0.87	0.00	0.14	0.00	0.20	0.00
Cr (VII)	-0.65	0.00	-0.14	0.00	-0.16	0.00
Cr (VIII)	0.47	0.00	0.08	0.00	0.08	0.00

A similar calculation has been performed for the system $Fe_{0.5}Co_{0.5}$/Cr(001) consisting of 1, 2, and 4 ML $Fe_{0.5}Co_{0.5}$/Cr(001) and the results are shown in Table 4. The Fe and Co on the deposited layer are ferrimagnetically coupled; also, the alternative Cr substrate layers are ferrimagnetically coupled. The magnitude of the Cr spin magnetic moments is decresing with the distance to the the Fe/Co interface.

The calculation results for the $Fe_{0.5}Co_{0.5}$/Cr(001) system consisting of 1, 2, and 4 ML of $Fe_{0.66}Co_{0.34}$/Cr(001) are shown in Table 5.

Table 4. The layer-resolved spin and orbital magnetic moments for the configuration consisting of 1, 2, and 4 ML of $Fe_{0.66}Co_{0.34}$/Cr(001).

Layer	6ML		4ML		2ML		1ML	
	$m_s(\mu_B)$	$m_l(\mu_B)$	$m_s(\mu_B)$	$m_l(\mu_B)$	$m_s(\mu_B)$	$m_l(\mu_B)$	$m_s(\mu_B)$	$m_l(\mu_B)$
Fe (VI)	2.85	0.13	-	-	-	-	-	-
Co (VI)	1.74	0.15	-	-	-	-	-	-
Fe (V)	2.43	0.07	-	-	-	-	-	-
Co (V)	1.64	0.09	-	-	-	-	-	-
Fe (IV)	2.55	0.06	2.86	0.14	-	-	-	-
Co (IV)	1.63	0.10	1.74	0.15	-	-	-	-
Fe (III)	2.51	0.03	2.43	0.06	-	-	-	-
Co (III)	1.64	0.10	1.64	0.09	-	-	-	-
Fe (II)	2.57	0.07	2.58	0.07	2.88	0.12	-	-
Co (II)	1.64	0.10	1.63	0.10	1.75	0.15	-	-
Fe (I)	2.00	0.05	1.98	0.05	1.80	0.05	2.28	0.09
Co (I)	1.03	0.07	1.03	0.07	1.31	0.07	0.22	0.03
Cr (I)	-0.30	0.00	-0.20	0.00	-0.64	0.00	-0.68	0.00
Cr (II)	0.25	0.00	0.17	0.00	0.41	0.00	0.51	0.00
Cr (III)	-0.20	0.00	-0.12	0.00	-0.40	0.00	-0.36	0.00
Cr (IV)	0.11	0.00	0.08	0.00	0.20	0.00	0.22	0.00

From the data presented in Tables 3, 4, and 5 we can summarize that Fe induces a ferrimagnetic behavior in the Cr substrate. The $Fe_{0.66}Co_{0.34}$ and $Fe_{0.5}Co_{0.5}$ alloy have the same influence on the substrate, but the magnitude of the Cr magnetic moments is suppressed with increasing the Co content in the deposited layer. Also, The Cr magnetic moments decrease by increasing the number of deposited Fe-Co layers.

In order to investigate the magnetic properties of the multilayers, we performed hysteresis loops between -1 and 1 T at temperatures between 4 and 300 K. Each hysteresis loop was recorded after field-cooling the sample from 300 K to the desired temeprature in

0.3 T. The cooling field of 0.3 T ensures that the $Fe_{65}co_{35}$ layer magnetization is saturated during cooling. The exchange bias field, H_E, and coercivity, H_C, were determined from the hysteresis loops and are defined as $H_E = (H_{RC} + H_{LC})/2$ and $H_C = (H_{RC} - H_{LC})/2$, respectively. H_{RC} and H_{LC} represent the right-hand and left-hand side coercive fields in the positive and negative field direction. A linear background was subtracted from the hysteresis loops due to the diamagnetic response of the Si/SiO_2 substrate. The magnetic measurement results are shown in Figure 9. For the multilayer sample with 102 nm of $Fe_{65}Co_{35}$, we can see no exchange bias, the hysteresis loops being symmetrical. The absence of exchange bias in this sample could be explained in terms of $Fe_{65}Co_{35}$ layer thickness, the dipolar interaction in the $Fe_{65}Co_{35}$ layer being stronger than the exchange interaction at the interface. This is further confirmed by the rather low coercivity value obtained for this sample at 4 K. For the sample with 52 nm of $Fe_{65}Co_{35}$ we have the onset of exchange bias, the hysteresis curve at 4 K being asymmetrical. After 40 K, the hysteresis curves become symmetrical, pointing to the fact that the exchange bias has vanished. The same behaviour was found for the multilayer sample with 25 nm of $Fe_{65}Co_{35}$, however, the exchange bias values and coercivity

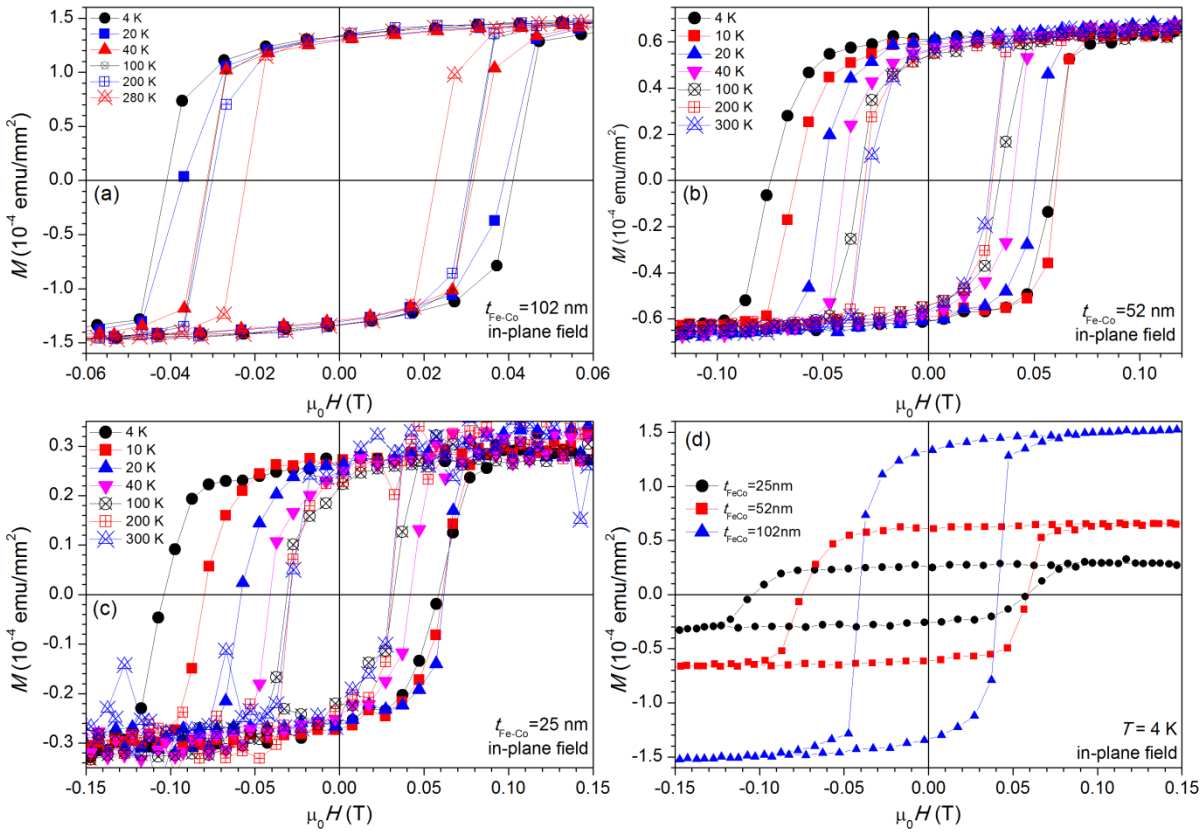

Figure 6. Hysteresis loops for the multilayer Cr/Fe-Co samples with a Fe-Co layer thickness, t_{FeCo}, of 25 (a), 52 (b), and 102 nm (c) respectively. In subfigure (d), the hysteresis loops at 4 K for all three multilayer samples are shown.

are higher than the other two samples at 4 K. The exchange bias field and coercivity values are summarized in Figure 10. The exchange bias field decreases with temperature and becomes zero around 40 K. This temperature is defined as the blocking temperature. This value is lower than previously reported results [7,8,20], probably due to the much larger thickness values of both the Cr and $Fe_{65}Co_{35}$ layers in our samples. The decrease of exchange bias with temperature can be explained by the fact that although Cr is antiferromagnetically ordered up to the Neel temperature, at temperatures higher than the blocking temperature, the interface coupling between Cr and FeCo spins become random due to thermal fluctuations [8,20]. The exchange bias values at 4 K decrease with increasing

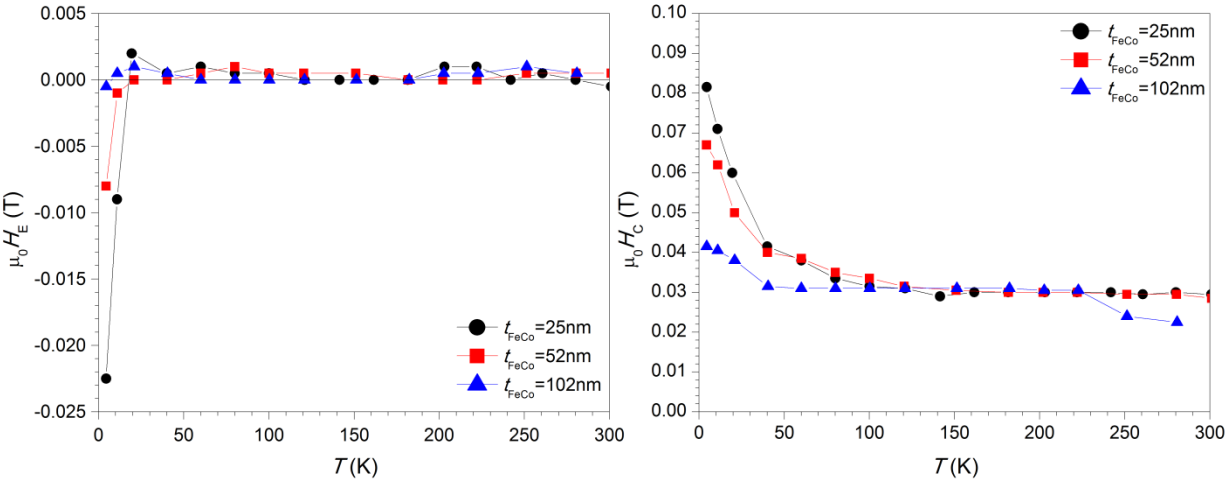

Figure 7. Exchange bias field (a) and coercivity (b) values for all three multilayer Cr/FeCo samples.

$Fe_{65}Co_{35}$ layer thickness, possibly due to the increased dipolar interaction and also due to a decreasing interface moment with increasing thickness, as was pointed out by band structure calculations. The maximum exchange bias value of 0.023 T for the sample containing 25 nm of $Fe_{65}Co_{35}$ is higher than previously obtained values [7,8,20]. The high exchange bias field values can be explained by the presence of interface disorder, which could lead to an uncompensated commensurate SDW in Cr at the interface [7,8,20].

The coercivity values decrease with temperature for all of the multilayer samples - Figure 10b. The coercivity values remain roughly unchanged at temperatures higher than 100 K and is independent of $Fe_{65}Co_{35}$ thickness between 100 and 300 K. The enhancement of coercivity could be attributed to exchange bias present in these samples. It is worthwhile to note that for the sample containing 102 nm of $Fe_{65}Co_{35}$, coercivity values are enhanced below 40 K. This could mean that a weak exchange bias is present in this sample, but cannot be observed in the hysteresis loops. Electronic structure calculations show that the increase of Co content in the ferromagnetic layer decreases the interface magnetic moment.

Also, the interface moment decreases with increasing the number of layers deposited on top of Cr.

2.2. Conclusions for Phase 2: January - December 2016

In Phase 2 we studied the effect of Ar pressure on the structural properties of hard magnetic Cr/Sm-Co multilayers and the effect of $Fe_{65}Co_{35}$ thickness on the structural, electronic and magnetic properties of soft magnetic Cr/$Fe_{65}Co_{35}$ bilayers.

Hard magnetic Cr(150 nm)/Sm-Co(30 nm)/Cr(5 nm) multilayers were prepared. It was found that higher Ar pressures leads to the formation of the Sm_2Co_{17} phase. The $SmCo_5$ phase can be obtained by depositing Sm-Co films at lower Ar pressures, followed by annealing at high temperature, around 900 ºC.

Soft magnetic Cr/$Fe_{65}Co_{35}$ bilayers were prepared in the configuration Cr(96 nm)/$Fe_{65}Co_{35}$(25-102 nm). XRD results show that the films are textured along the (110) direction, while XRR measurements showed the presence of a rough interface. Magnetic measurements showed that the onset of exchange bias happens at around 52 nm of $Fe_{65}Co_{35}$, however, the presence of a weak exchange bias is possible for a $Fe_{65}Co_{35}$ thickness of 102 nm. The exchange bias field values increase with decreasing $Fe_{65}Co_{35}$ thickness and disappears around 40 K. Coercivity also increases with decreasing $Fe_{65}Co_{35}$ thickness and decreases with temperature. This behavior was attributed to the interface exchange coupling. Electronic structure calculations showed a decreasing interface moment with increasing Co content in the Fe-Co layer at the interface. The interface moment was also found to decrease with increasing the number of deposited Fe-Co layers.

The results obtained through the activities outlined in the project were submitted for publication in ISI indexed articles [1,2] and presented at international conferences [3-6]. The fact that the young PhD students involved in the project participated at international conferences is very important in that it contributes to their formation as future researchers. The exchange coupling in hard/soft multilayer systems will be studied in Phase 3, which will begin in January 2017.

2.3. References

[1] S. Mican, D. Benea, A. Takacs, O. Isnard, V. Pop, *"Influence of the $Fe_{65}Co_{35}$ Thickness on the Structural, Electronic and Magnetic properties of Cr/$Fe_{65}Co_{35}$ bilayers"*, paper to be submitted to *Thin Solid Films.*

[2] R. Hirian, S. Mican,O. Isnard, L. Barbu-Tudoran, V. Pop, *"Influence of Microstructure on the Interphase Exchange Coupling of $Nd_2Fe_{14}B$+10wt%α-Fe Nanocomposites Obtained at Different Milling Energies",* paper submitted to *Journal of Alloys and Compounds.*

[3] S. Mican, R. Hirian, O. Isnard, V. Pop, *"The Influence of Short Time Heat Treatment on the Microstructure and Magnetic Behavior of the $SmCo_5$/α-Fe Nanocomposite Obtained by Mechanical Milling"*, poster presented at the 8th Joint European Magnetic Symposia (JEMS), 21st-26th August 2016, Glasgow, UK.

[4] S. Mican, D. Benea, A. Takacs, V. Pop, *"Structural and Magnetic Properties of Cr/$Fe_{65}Co_{35}$ Thin Films"*, poster presented at the 11th International Conference on Physics and Advanced Materials, 8th-14th September 2016, Cluj-Napoca, Romania.

[5] R. Hirian, S. Mican, O. Isnard, L. Barbu-Tudoran, "Effect of Starting Powder Premixing on the Interphase Exchange Coupling in $Nd_2Fe_{14}B$+10wt%Fe Nanocomposites Obtained Trough Mechanical Milling", oral presentation at the 16th International Balkan Workshop on Applied Physics and Materials Science, 7th-9th July 2016, Constanţa, Romania.

[6] R. Hirian, S. Mican,O. Isnard, L. Barbu-Tudoran, V. Pop *"Influence of Microstructure on the Interphase Exchange Coupling of $Nd_2Fe_{14}B$ + 10 wt%Fe Nanocomposites Obtained by Mechanical Milling"*, poster presented at the 24th International Workshop on Rare-Earth and Future Permanent Magnets and Their Applications (REPM 16), 28th August - 1st September 2016, Darmstadt, Germany.

[7] F. Y. Yang, C. L. Chien, *J. Appl. Phys.*, **93**, 6829-6831 (2003).

[8] J. S. Parker, L. Wang, K. A. Steiner, P. A. Crowell, C. Leighton, Phys. Rev. Lett. **97**, 227206 (2006).

[9] E. Fawcett, *Rev. Mod. Phys.* **60**, 209 (1988).

[10] S. A. Werner, A. Arrot, H. Kendrick, *Phys. Rev.*, **155**, 528 (1957).

[11] M. N. Baibich et al., *Phys. Rev. Lett.,* **61**, 2472 (1988).

[12] P. Grünberg et al., *Phys. Rev. Lett.,* **57**, 2442 (1986).

[13] W. H. Meiklejohn, C. P. Bean, *Phys. Rev.*, **102**, 1413-1414 (1956).

[14] J. Nogués, I. K. Schuller, *J. Magn. Magn. Mater.*, **192**, 203 (1999).

[15] V. Skumryev, S. Stoyanov, Y. Zhang, G. Hadjipahayis, D. Givord, J. Nogués, *Nature (London)*, **423**, 850 (2003).

[16] C. Chappert, A. Fert, F. N. van Dau, *Nature Mater.*, **6**, 813 (2007).

[17] L. Anghinolfi, F. Bisio, M. Canepa, L. Mattera, *Phys. Rev.* B, **81**, 224427 (2010).

[18] D. Aernout, C. L'abbé, M. Rots, H. Fritzsche, J. Meersschaut, *Phys. Rev.* B, **73**, 134419 (2006).

[19] K. Kim, S. Shin, *J. Kor. Phys. Soc.* **54**, 175-179 (2009).

[20] Y. C. Feng, D. E. Laughlin, D. N. Lambeth, *J. Appl. Phys.*, **76**, 7311-7316 (1994).

[21] H. Ebert, D. Koedderitzsch, J. Minar, *Rep. Prog. Phys.,* **74**, 096501 (2011).

[22] R. Zeller et al., *Phys. Rev.* B, **52**, 8807 (1995).

[23] S. H. Vosko, L. Wilk, M. Nusair, *Can. J. Phys.*, **58**, 1200 (1980).